Palaeogeography, Palaeoclimatology, Palaeoecology 510 (2018) 78–92

Contents lists available at ScienceDirect

Palaeogeography, Palaeoclimatology, Palaeoecology

journal homepage: www.elsevier.com/locate/palaeo

# High-resolution astrochronological record for the Paleocene-Oligocene (66–23 Ma) from the rapidly subsiding Bohai Bay Basin, northeastern China

Zhanhong Liu[a,b], Chunju Huang[c,*], Thomas J. Algeo[c,d,e,**], Huimin Liu[f], Yunqing Hao[f], Xuebin Du[a], Yongchao Lu[a], Ping Chen[a], Laiyuan Guo[a], Li Peng[a]

[a] College of Marine Science and Technology, China University of Geosciences, Wuhan 430074, China
[b] First Institute of Oceanography, State Oceanic Administration, Qingdao 266061, China
[c] State Key Laboratory of Biogeology and Environmental Geology, School of Earth Sciences, China University of Geosciences, Wuhan 430074, China
[d] State Key Laboratory of Geological Processes and Mineral Resources, China University of Geosciences, Wuhan 430074, China
[e] Department of Geology, University of Cincinnati, Cincinnati, OH 45221-0013, USA
[f] Geological Scientific Research Institute, Shengli Oilfield Company of SINOPEC, Dongying 257015, China

ARTICLE INFO

*Keywords:*
Paleogene
Astronomical time scale
Orbital forcing
Lacustrine facies
Basin subsidence
Time series analysis

ABSTRACT

The Paleogene succession of the Bohai Bay Basin (BBB), a highly productive petroleum basin in northeastern China with predominantly lacustrine fill, is poorly dated at present. Here, we generated an internal astronomical time scale (ATS) for the Paleogene strata of the Bohai Bay Basin (Dongying Depression, Jiyang Subbasin) using multitaper method (MTM) spectral analysis of high-resolution gamma ray logs. This ATS, which extends from 66 to 23 Ma, is anchored to the standard geologic time scale by calibration to the Paleogene/Neogene boundary (23.03 Ma) at the top of Dongying Formation. Based on this ATS, we recalibrated the ages of biozones, rifting episodes, and paleoclimate stages within the BBB. The recalibrated ages of rifting episodes and related fluctuations in sedimentation rates exhibit a close relationship to secular variation in production rates of Pacific oceanic plateaus and spreading rates of the Southeast Indian Ridge, confirming that the subsidence history of the BBB was significantly influenced by subduction of the Pacific Plate along the eastern margin of Asia and by collision of the Indian and Eurasian plates. Age recalibration also facilitated re-evaluation of the relationship of sedimentation in the Bohai Bay Basin to the Paleogene climate history of East Asia, e.g., confirming a cooling and drying trend throughout the Eocene.

## 1. Introduction

The Bohai Bay Basin (BBB) is the most productive petroleum basin in China, accounting for nearly one-third of the total annual oil production of ~1.34 × $10^3$ million barrels in China (Hao et al., 2009). The Paleogene succession of the BBB, which comprises > 50% of total basin fill, is relatively poorly dated at present. Although key sections have been studied biostratigraphically, providing broad age assignments for the major stratigraphic units, absolute age constraints are based exclusively on K-Ar dates for nine volcanic ash layers in the Liaohe Subbasin and paleomagnetic dating of $Es^3$ (i.e., the 3rd Member of the Shahejie Formation) in the Jiyang Subbasin (Yao et al., 1994, 2007). However, Yao et al. (1994) provided little information on their methodology and no estimates of age uncertainties, making the reported dates of limited value. This lack of documentation is troubling in view of the well-known analytical difficulties in applying the K-Ar radioisotope method (Min et al., 2000; Kuiper et al., 2008). Consequently, the present geochronological framework for the Paleogene BBB is of low resolution and uncertain validity, despite its widespread use (e.g., Hao et al., 2009; Feng et al., 2013).

Astrochronology provides a method for developing highly detailed internal time scales in poorly dated successions, provided that continuous sedimentary records are available. This technique relies on spectral identification of Earth's orbital periodicities from the 405-kyr long-eccentricity cycle to the ~21-kyr precession cycle, i.e., the "Milankovitch band" (e.g., Preto and Hinnov, 2003; Strasser et al., 2006; Ruhl et al., 2010; Hinnov and Hilgen, 2012). Lacustrine strata in continental rift basins are particularly suitable for high-resolution cyclostratigraphic analysis to establish astronomical time scales owing to continuous sedimentation at high average rates in climatically sensitive settings. Previous studies have shown that orbital-scale climate cycles are well-preserved in lacustrine or marginal-marine successions of the

* Corresponding author.
** Correspondence to: T. J. Algeo, State Key Laboratory of Geological Processes and Mineral Resources, China University of Geosciences, Wuhan 430074, China.
*E-mail addresses:* huangcj@cug.edu.cn (C. Huang), thomas.algeo@uc.edu (T.J. Algeo).

https://doi.org/10.1016/j.palaeo.2017.10.030
Received 16 July 2017; Received in revised form 23 September 2017; Accepted 30 October 2017
Available online 31 October 2017
0031-0182/ © 2017 Elsevier B.V. All rights reserved.

Upper Triassic-Lower Jurassic Newark Basin in eastern North America (Olsen and Kent, 1996), the Upper Cretaceous Songliao Basin in northeastern China (Wu et al., 2009), the Eocene Green River Basin in western North America (Machlus et al., 2008), and Miocene basins around the Mediterranean Sea (Abels et al., 2010).

In this study, we undertake a cyclostratigraphic analysis of lacustrine deposits of Paleogene age from the Dongying Depression of the BBB, using continuous natural gamma-ray log profiles as a basis for spectral analysis and high-resolution XRF core-scanner data to investigate the lithologic and mineralogic controls on gamma-ray variation. The goals of this study are to (1) construct a high-resolution astronomical time scale (ATS) for the full Paleogene succession of the BBB, (2) use this ATS to refine the ages of biozones, rifting episodes, and paleoclimate stages within the BBB, and (3) evaluate the subsidence and sedimentation history of the BBB in relation to regional tectonic and climatic events. These results significantly refine the geochronological framework of the BBB, provide new insights into basin evolution, and demonstrate its connections to climatic and tectonic events of Paleogene East Asia.

## 2. Geological background

### 2.1. Structure and evolution of the Bohai Bay Basin

The Bohai Bay Basin (BBB) is a Cenozoic rift basin formed on the basement of the North China Craton, covering an area of ~200,000 km$^2$ (Fig. 1A) (Li et al., 2014). Its tectonic evolution comprises a Paleogene syn-rift stage and a Neogene-Quaternary post-rift stage (Guo et al., 2012). The syn-rift stage was characterized by extension and rifting, resulting in a series of grabens and half grabens developed along NW- and NE-trending faults (Qi and Yang, 2010). Regional extension was terminated at the end of the Oligocene, and since the early Miocene the BBB has subsided as a unit due to post-rift thermal subsidence (Guo et al., 2012).

Several hypotheses have been advanced concerning the origin of the BBB, including (1) subduction and rollback of the Pacific Plate along the eastern margin of Asia (Northrup et al., 1995), (2) upwelling of hot mantle material beneath the basin (Qi and Yang, 2010), (3) eastward displacement (or "escape") of basement crust due to collision of the Indian and Eurasian plates (Tapponnier et al., 1982), or (4) combinations of the above mechanisms (Liu et al., 2004; Chen et al., 2017). Evaluating these mechanisms has proven difficult in part due to insufficiently precise information regarding the age of subsidence events within the BBB.

### 2.2. Stratigraphic framework and depositional systems of Dongying Depression

The Jiyang Subbasin is the most petroliferous area in the BBB, with an annual production of ~195 million barrels of oil in 2000. It is subdivided into four depressions, of which the 5700-km$^2$ Dongying Depression, located on the southern margin of the Jiyang Subbasin, is the focus of the present study (Fig. 1B; Feng et al., 2013). It is further subdivided by a series of en echelon normal faults into four local basins: the Minfeng, Lijin, Niuzhuang, and Boxing sags (Feng et al., 2013). The boreholes used in this study are located in the Lijin Sag (Shengke-1 and He-166) and the Niuzhuang Sag (Niuye-1 and Niu-38) (Fig. 1C).

The Dongying Depression records both Paleogene syn-rift and Neogene post-rift stages (Lin et al., 2004). The syn-rift succession comprises > 7000 m of mainly lacustrine sediments and the post-rift succession 1000–2000 m of mainly fluvial sediments (Zhang, 2004). The syn-rift succession contains the Kongdian (Ek), Shahejie (Es), and Dongying (Ed) formations, each of which is divided into several members (Fig. 2; Petroleum Geology Group of Shengli Oilfield, 1993;

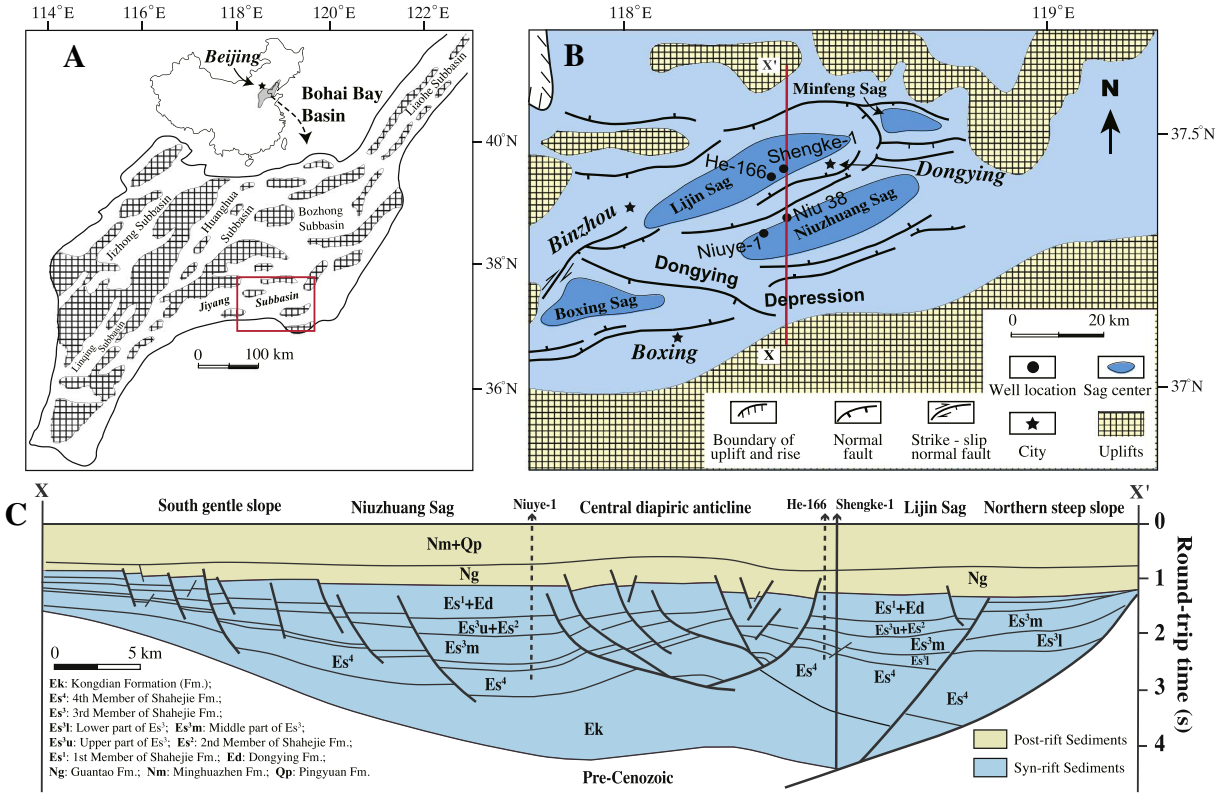


**Fig. 1.** (A) Structural map of the Bohai Bay Basin, showing location of the Dongying Depression of the Jiyang Subbasin (rectangle) (after Zhang, 2004). (B) Structural map of the Dongying Depression showing locations of the study wells and cross-section X-X′ (after Feng et al., 2013). (C) Structural cross-section across the Dongying Depression based on seismic profiles (after Feng et al., 2013). Burial depth is proxied by round-trip travel time. Abbreviations: Ek, Kongdian Formation (Fm.); Es$^4$, Es$^3$, Es$^2$, and Es$^1$, fourth to first members of Shahejie Fm.; Ed, Dongying Fm.; Ng, Guantao Fm.; Nm, Minghuazhen Fm.; Qp, Pingyuan Fm.

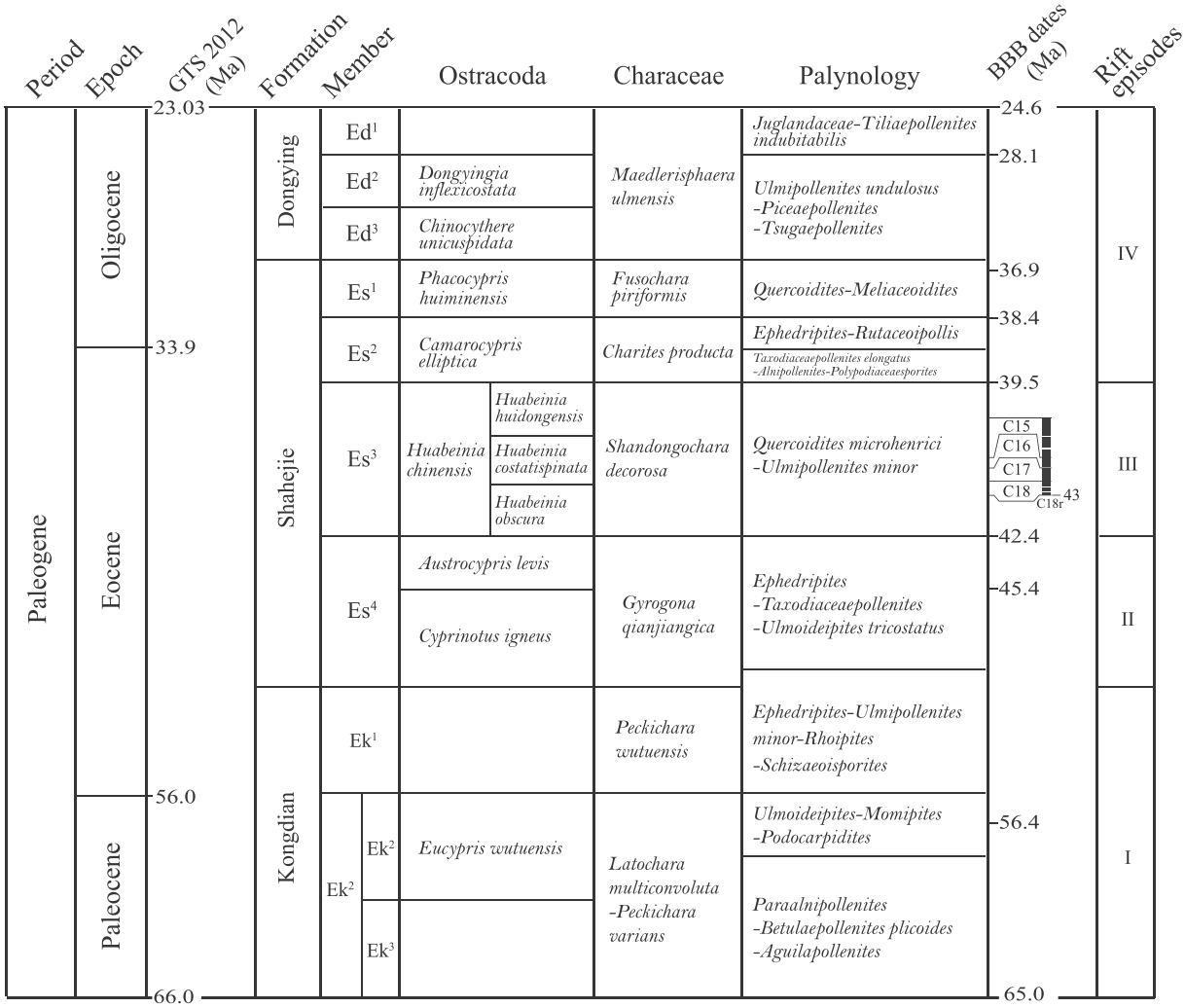


**Fig. 2.** Stratigraphic chart and timescales for the Bohai Bay Basin. The ages at left are based on the GTS2012, whereas those on the right are from Yao et al. (1994). The Ostracoda, Characeae, and palynological biozones are from RIPEDPCI (1978a, 1978b, 1978c). The rifting episodes are after Hao et al. (2009) and Feng et al. (2013).

**Table 1**
Lithologies of stratigraphic units in Shengke-1 drillcore.[a]

| Formation | Member | Units | Lithology |
|---|---|---|---|
| Dongying | | | Coarse- to fine-grained sandstone interbedded with mudstone |
| Shahejie | $Es^1$ | Upper | Sandstone interbedded with gray mudstone |
| | | Middle | Gray mudstone and shale with thin limestone interbeds |
| | | Lower | Sandstone interbedded with green and gray mudstone |
| | $Es^2$ | | Conglomerate and sandstone interbedded with purple to red mudstone. |
| | $Es^3$ | Upper-Middle | Fine- to coarse-grained sandstone interbedded with gray and green mudstone |
| | | Lower | Gray to dark mudstone and oil shale |
| | $Es^4$ | Upper | Gray mudstone, oil shale intercalated with sandstone, and thin-bedded limestone |
| | | Lower | Alternating layers of red sandstone and mudstone interbedded with evaporite deposits |
| Kongdian | $Ek^1$ | | Alternating layers of gypsum, red sandstone, and gray mudstone |
| | $Ek^2$ | Upper | Alternating layers of gray mudstone, oil shale, and medium- to fine-grained sandstone |
| | | Lower | Conglomerate and coarse sandstone interbedded with purple to red mudstone |

[a] After Feng et al. (2013) and Li et al. (2014).

Feng et al., 2013). The rift history of the depression is subdivided into four episodes: (I) "Early-initial rifting" (Ek Formation) from Early Paleocene to Early Eocene, (II) "Late-initial rifting" ($Es^4$ Member) from Early Eocene to Middle Eocene, (III) "Climax rifting" ($Es^3$ Member) from Middle Eocene to Late Eocene, and (IV) "Late rifting" ($Es^2$ Member to Ed Formation) from Late Eocene to Late Oligocene. Deposits of the first rifting episode unconformably overlie pre-Cenozoic strata, and those of the final episode are overlain by post-rift strata that are variably conformable (mainly in the basin depocenter) to unconformable (mainly on the basin margins) (Feng et al., 2013). The Shengke-1 (SK-1) drillcore penetrated the entire Paleocene interval of the Dongying Depression; a summary of the lithologies in each stratigraphic unit is shown in Table 1.

Six depositional systems were identified in the $Es^3$ and lower $Es^2$ members of the Dongying Depression through analysis of drillcores, well logs, and seismic data (Feng et al., 2013): (i) proximal fan-delta

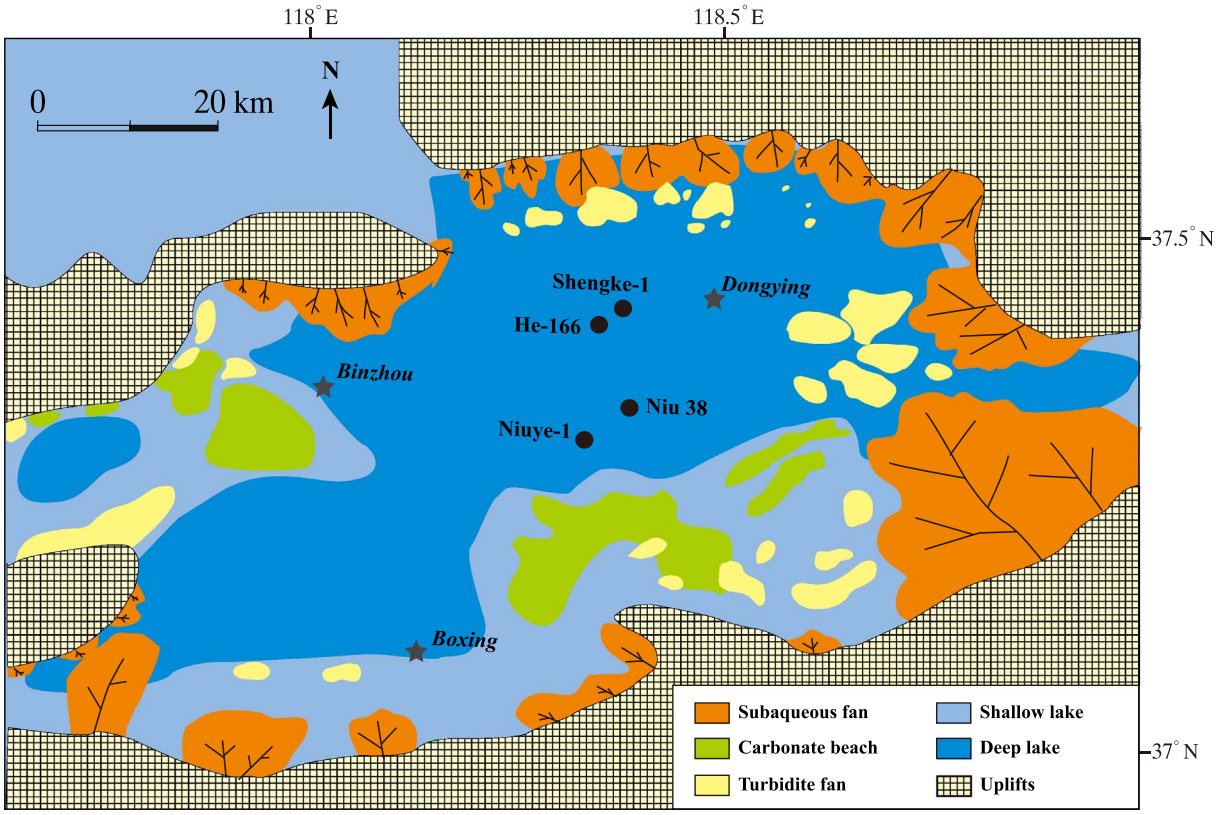


**Fig. 3.** Facies distribution during deposition of the lower $Es^3$ Member in the Dongying Depression (after Feng et al., 2013, and Zhang, 2004).

deposits along the northern faulted margin, (ii) braided-delta deposits along the southern gentle slope margin, (iii) fluvial delta deposits with westward paleocurrents along the long axis of the depression, (iv) shallow-lake deposits on the western and southern ramp slopes, (v) incised-valley fill and sub-lacustrine fan deposits on the southern slope margin, and (vi) deep-lake fine-grained deposits in the basin depocenter. The present study drillcores are located near the center of the Dongying Depression, generally representing deep-lake or pro-delta environments (Fig. 3). In addition to the detrital deposits, the $Ek^1$ and lower $Es^4$ members contain four intervals of gypsum and halite deposits, which are interbedded with calcareous mudstone and black shale, documenting episodic development of saline-lake and salt-flat environments (Li et al., 2014).

### 2.3. Existing age control and stratigraphic hiatuses in Dongying Depression

The existing chronostratigraphic framework of the BBB is based on a combination of radiometric and paleomagnetic dating as well as paleontological correlations (RIPEDPCI, 1978a, 1978b, 1978c; Yao et al., 1994, 2007). Yao et al. (1994) dated volcanic layers in the Liaohe Subbasin using the K-Ar method, yielding nine ages ranging from 65.0 Ma at the base of the Ek Formation to 24.6 Ma at the top of the Ed Formation (Fig. 2). Yao et al. (1994) also measured the paleomagnetism of 430 samples from the 2270–3307 m interval in the Niu-38 drillcore of the Dongying Depression, corresponding to the middle and lower $Es^3$ Member, and correlated their magnetic reversal record to C15n-C19r of the geomagnetic polarity time scale of Harland et al. (1982). Yao et al. (2007) recalculated the age for the C18n.1r/C18n.1n reversal at 3236 m in the Niu-38 core to 38.975 Ma, according to Ogg and Smith (2005). The present age framework of the BBB is based on the integration of these radiometric and geomagnetic polarity age constraints with litho-, seismo-, and palynostratigraphic correlations between different subbasins (Fig. 2; Hao et al., 2009; Feng et al., 2013).

The syn-rift Paleogene succession of the Dongying Depression is considered to be fully conformable, i.e., deposited continuously without identifiable hiatuses (Fig. 2). Based on a duration of ~43 Myr (i.e., ~66–23 Ma; Gradstein et al., 2012), the 5600-m-thick Paleogene syn-rift succession in the SK-1 drillcore accumulated at an average rate of ~130 m $Myr^{-1}$. The only known unconformity is at the base of the succession, separating syn-rift deposits from underlying pre-Cenozoic basement rocks. The temporal gap between the Cretaceous/Paleogene boundary and the base of the lowermost Paleocene strata in the Dongying Depression is short, as shown by both biostratigraphic and lithostratigraphic considerations. *Paraalnipollenites* and *Betulaepollenites* are characteristic taxa of the early Paleocene in the northern and northeastern China palynofloristic regions (Song, 1999; Hao et al., 2010; Wang et al., 2010). In the SK-1 drillcore of the Dongying Depression, the early Paleocene biozone *Paraalnipollenites-Betulaepollenites plicoides-Aguilapollenites* has a thickness of ~1405 m, suggesting that most or all of the lower Paleocene is present (Fig. 2). The second argument for a limited hiatus in the earliest Paleocene is that astronomical tuning of the composite gamma-ray profile yields 405-kyr cycles dating back to 65.56 Ma, or within ~0.5 Myr of the Cretaceous/Paleogene boundary (see Section 5.1). The top of the Dongying Formation, corresponding to the Paleogene/Neogene boundary, represents a regional unconformity surface in the BBB (Feng et al., 2013; Huang et al., 2014). It is unconformable around the margins of the Dongying Depression but conformable in its center (where the Shengke-1 borehole is located), as shown by analysis of seismic and fission track data (Wu et al., 1998). These considerations support our inference that syn-rift sedimentation in the Dongying Depression began soon after the Cretaceous/Paleogene transition (at 66.0 Ma) and continued uninterrupted to the Paleogene/Neogene transition (at 23.03 Ma).

## 3. Materials and methods

### 3.1. Samples and core logging

Gamma ray (GR) profiles can reflect changes in the amounts of clay minerals, which commonly contain substantial K and Th, and organic matter, which readily adsorbs U. As the fluxes of clay minerals and organic matter to lake basins is generally sensitive to environmental and climatic conditions, GR curves can preserve signals related to climate periodicity (e.g., Prokoph et al., 2001; Schnyder et al., 2006; Wu et al., 2014). Typically, warm and humid intervals are associated with increased clay-mineral and organic inputs, leading to higher GR values, whereas cool and dry intervals have reduced inputs that yield lower GR values. Climate variation at intermediate timescales ($\sim 10^4$–$10^6$ yr; i.e., Milankovitch-band periodicities) is driven mainly by variations in the Earth's orbital configuration, with eccentricity maxima creating the potential for large variations in the seasonality of insolation, and eccentricity minima limiting variation in the seasonality of insolation (Postma and Ten Veen, 1999; Van Vugt et al., 2001).

In this study, we generated a composite gamma ray profile from the gamma-ray records for the He-166 and Shengke-1 (SK-1) boreholes, which are located in the north-central area of the Dongying Depression (Fig. 1B). The He-166 borehole (37.43°N, 118.42°E) was drilled in 2001 and the SK-1 borehole (37.45°N, 118.47°E) in 2007, just ~3 km to the northeast of He-166. The SK-1 borehole has a total depth of ~7025 m, making it the deepest borehole in eastern China to date. Our composite GR profile joins the upper part of the He-166 GR log (i.e., top of Ed to base of $Es^3$ interval; 1245–3423 m, thickness of 2178 m) with the lower part of the SK-1 GR log (i.e., top of $Es^4$ Member to base of Ek Formation; 2922–7005.5 m, thickness of 4083.5 m). The resulting composite GR profile has a total thickness of 6261.5 m and represents a continuous record through the entire Paleogene succession of the Dongying Depression (Fig. 4). The main reason that we did not make use of the GR record of the deep SK-1 borehole alone was that this borehole transects a fault that cut out ~64 m of the lower $Es^3$ Member (Fig. 1C). In addition, the He-166 profile offers superior stratigraphic resolution for the Ed to $Es^3$ interval, which is ~40% thicker than the correlative interval of the SK-1 profile. There is no uncertainty about the stratigraphic equivalence of the tiepoint in these two boreholes because it represents the contact between the $Es^4$ and $Es^3$ Members of the Shahejie Formation, at which there is a lithologic change from evaporites to silty mudstones linked to regional climate change. It should be noted that the two boreholes are only ~3 km apart and exhibit very similar GR patterns despite differences in the thicknesses of correlative intervals; indeed, their general similarity was the basis for recognition of a ~64-m gap in the SK-1 GR profile.

We also made use of a drillcore from a third borehole, Niuye-1 (37.33°N, 118.40°E), which was drilled in 2012 in the south-central area of the Dongying Depression (Fig. 1B). This borehole was cored at 3295–3497 m (upper $Es^4$ and lower $Es^3$ members) with a ~92% recovery rate, and the drillcore was subsequently scanned using an ITRAX instrument to generate concentration data for 44 elements at a high (0.004-m) spatial resolution. This drillcore exhibits pervasive meter-scale sedimentary cyclicity, as seen in a representative 21.0-m-thick interval from the upper $Es^4$ Member (Fig. 5). A fourth borehole, Niu-38 (37.36°N, 118.48°E), which was drilled in 1988 in the central area of the Niuzhuang Sag (Fig. 1B), was not analyzed in this study but served as the source of geomagnetic polarity data that was used in earlier geochronological studies of the BBB stratigraphic succession (Yao et al., 1994, 2007).

### 3.2. Geochemical analyses

Two sets of core samples were collected from 21.0-m-thick interval of the upper $Es^4$ Member in Niuye-1 drillcore. The first set, for TOC (total organic carbon) analysis, consisted of 25 samples with an average sample spacing of 0.8 m. The second set, for mineral composition analysis, consisted of 96 samples with an average sample spacing of 0.22 m. For each sample, about 10 g of fresh rock was crushed to powder finer than 200-mesh size using a steel jaw crusher.

TOC analyses were carried out in the Experimental Research Center (ERC) of the Geological Scientific Research Institute of Shengli Oilfield of SINOPEC. About 200 mg of sample powder was weighed and treated with 10% hydrochloric acid at 60 °C to remove carbonate, and then washed with distilled water to remove remaining HCl. Afterwards, the residue was dried and analyzed using a CS-600 analyzer. Instrumental accuracy is ± 2% of reported TOC values, based on replicate analyses of the Chinese National Standard GB/T 19145–2003.

Mineralogical analyses were carried out by X-ray diffraction (XRD) using a Panalytical X′ Pert PRO MPD at the same facility (ERC). Powdered samples were placed in holders and scanned from 5° to 90° for whole-rock composition, and from 3° to 30° for the clay fraction, with both runs performed at 2° $min^{-1}$ with a step width of 0.02°, using CuKα radiation and a graphite monochromator. The accuracy of goniometer measurement is better than 2% based on replicate analyses of Chinese national standards SY/T6201-1996 and SY/T5163-1995.

### 3.3. Time-series analysis

The composite GR profile from the He-166 and SK-1 boreholes was analyzed with the multitaper method (MTM) spectral estimator (Thomson, 1982) using the SSA-MTM Toolkit (Ghil et al., 2002) with robust red noise models (Mann and Lees, 1996). Time-series analysis made use of the Gauss bandpass filtering function in the Analyseries 2.08 software (Paillard et al., 1996) in order to extract the short- and long-eccentricity cycles. All series were prewhitened by subtracting a 15% weighted average (in Kaleida Graph 4.1.3) to remove the long-term trends before undertaking spectral analysis. The nominal astronomical model La2010d (Laskar et al., 2011) was used to compare with the astronomically tuned composite GR record.

## 4. Results

### 4.1. Characteristics and origin of sedimentary cycles

The 21.0-m interval of the upper $Es^4$ Member of the Shahejie Formation in the Niuye-1 drillcore selected for investigation of sedimentary cyclicity exhibits regular variation of core image color between light and dark gray, comprising 10 cycles (C1-C10; Fig. 5). The individual cycles have thicknesses of 1.6 to 2.5 m (mean 2.05 ± 0.3 m) and, thus, are about half as thick as the cycles in the full $Es^4$ member of the SK-1 drillcore (3.3 to 4.3 m per cycle; see Section 4.2). This difference reflects in part different sedimentation rates in the Niuzhuang and Lijin Sags, in which the Niuye-1 and SK-1 boreholes are respectively located (Fig. 1B), and in part differences in lithology between the full $Es^4$ Member, which is dominated by evaporites, and the 21.0-m interval of the upper $Es^4$ Member studied for cyclicity (Fig. 5), which represents an oil shale interval in Niuzhuang Sag (Fig. 6) deposited at a lower average sedimentation rate.

Most core log and geochemical profiles for the Niuye-1 drillcore show variations that correspond closely to C1-C10. Relative to the lighter layers, the darker layers are enriched in TOC (3.7% vs 2.4%), quartz (35% vs 24%), and clay minerals (28% vs 16%), and depleted in calcite (22% vs 50%) (Fig. 5). Most of the XRF-scanned elements and elemental ratios also show a positive affinity to either the darker layers (e.g., Fe, Ti, S, V/Cr, and CIA) or the lighter layers (e.g., Ca), although the Mn profile does not match either closely (Fig. 5; Table 2). Because the GR profile is a wireline record, its downhole depths can be influenced by self-gravity, friction, mud pressure, and temperature variations in the borehole, resulting in limited uncertainty (< 1 m) about its correlation to the drillcore records. We used cross-correlation analysis of the GR and calcite records to determine the optimal correlation,

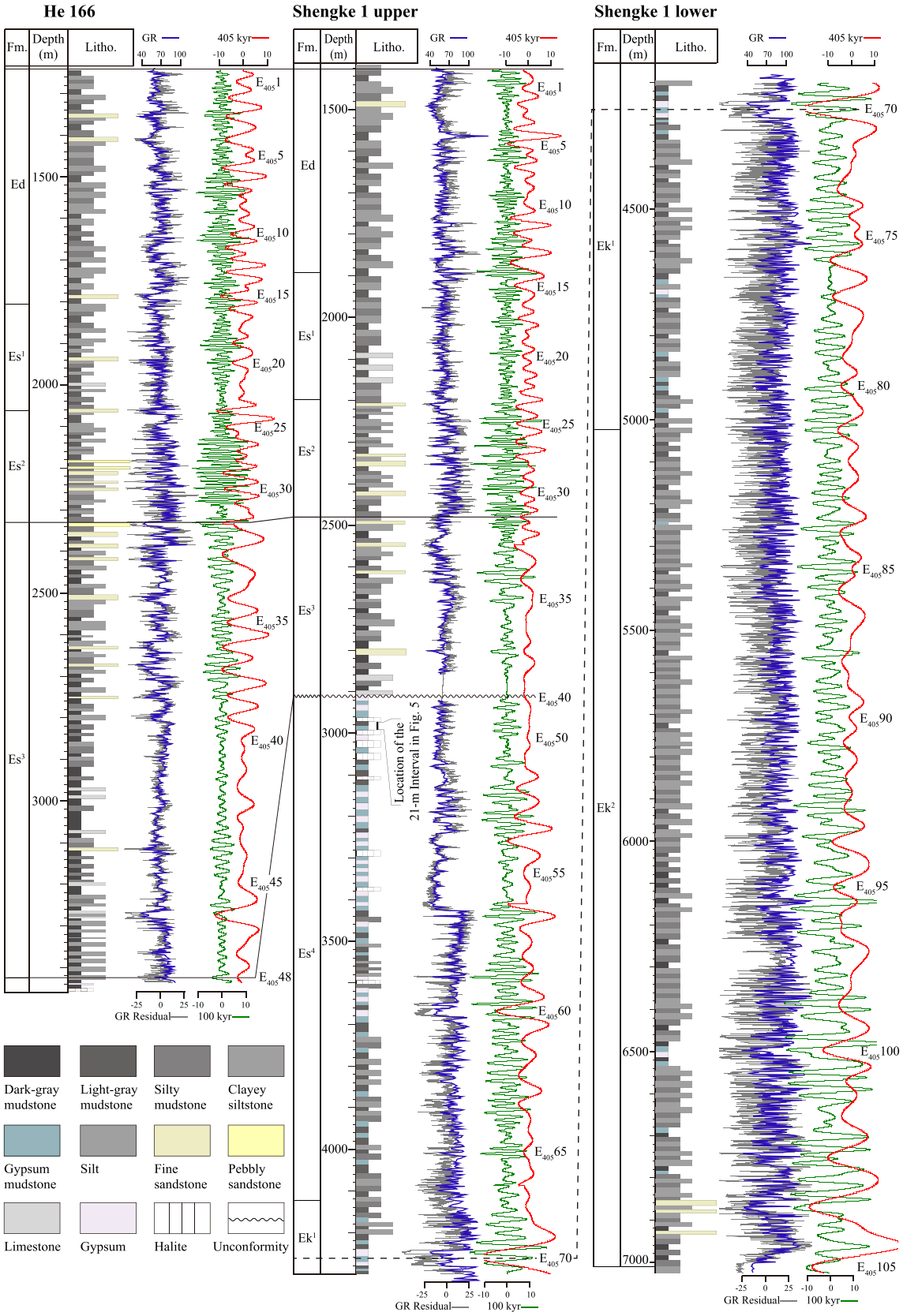


**Fig. 4.** High-resolution gamma ray logs and untuned filtered profiles for the He-166 and SK-1 boreholes. There is a gap in the lower $Es^3$ Member of SK-1 comparing with the $Es^3$ Member of He-166. In the uppermost part of $Es^4$ Member of SK-1 shows the relative location of 21-m interval of Niuye-1 drillcore for Fig. 5.

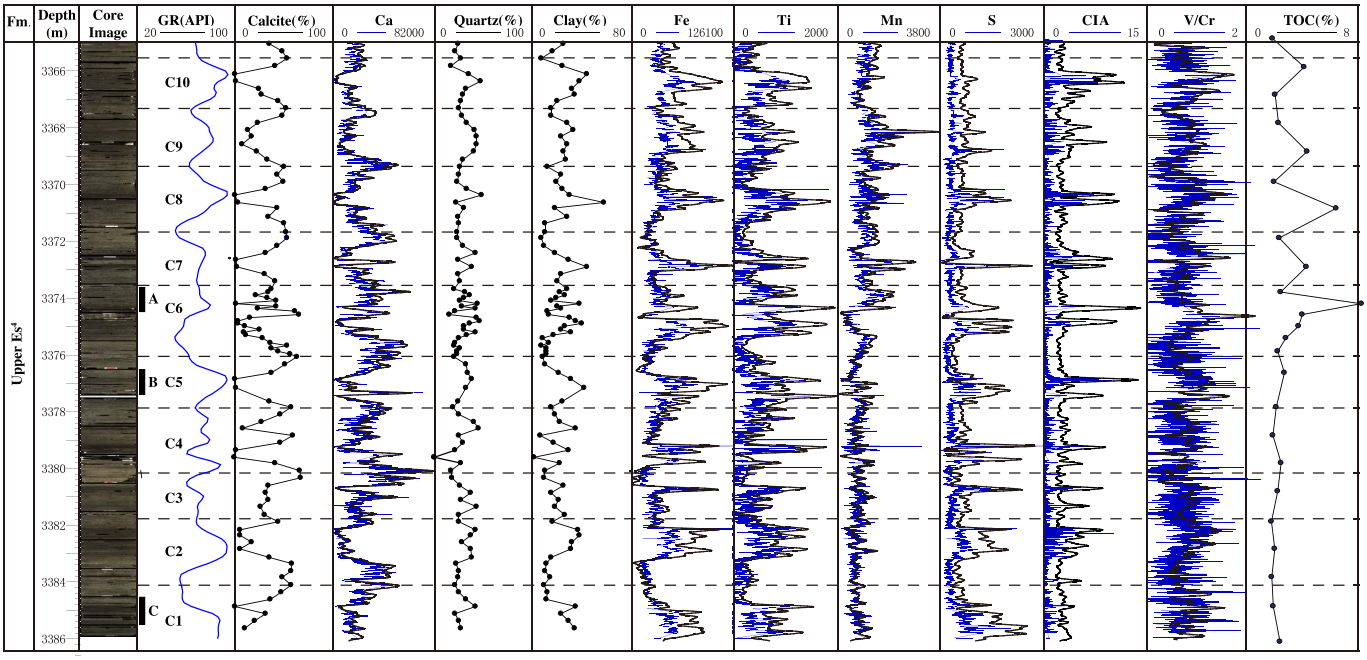


**Fig. 5.** Geochemical data for a 21.0-m interval in the upper $Es^4$ Member of the Shahejie Formation in the Niuye-1 drillcore exhibiting pronounced sedimentary cyclicity. The locations of core images A, B, and C (Fig. 6) are shown to the right of the lithologic column. GR, gamma ray; mineral fractions (calcite, quartz, and clay) are based on XRD; elemental concentrations are based on ITRAX scanning (units = counts) (Hennekam and Lange, 2012). The CIA (Chemical Index of Alteration) was used to evaluate climate and weathering conditions, and was calculated as CIA = $Al_2O_3/(Al_2O_3 + CaO^* + K_2O) \times 100$, where CaO* is the non-carbonate CaO fraction (Nesbitt and Young, 1982; Price and Velbel, 2003). The CIA profile in this study shows relative changes (not absolute values) of this proxy.

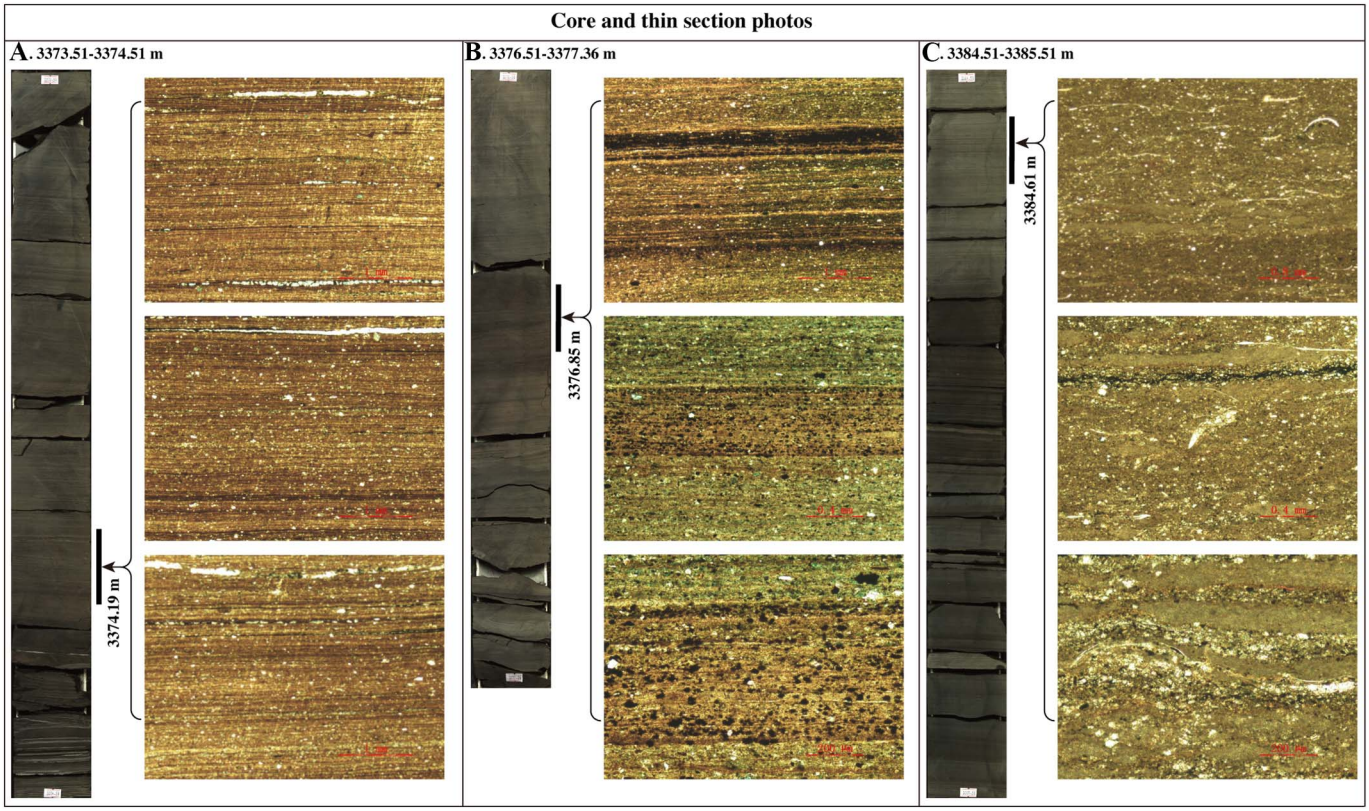


**Fig. 6.** Detailed core images and thin section photos. The location of core intervals A, B, and C are shown in Fig. 5. Thin section photos A and B are from darker layers, which show well-preserved lamination, and those for C are from lighter layers, which show bioturbation.

**Table 2**
Correlation coefficients among elements in Niuye-1 drillcore.[a]

| | Ca | Fe | Ti | S | Mn | CIA | V/Cr |
|---|---|---|---|---|---|---|---|
| Ca | 1 | | | | | | |
| Fe | -0.65 | 1 | | | | | |
| Ti | -0.61 | 0.76 | 1 | | | | |
| S | -0.49 | 0.69 | 0.53 | 1 | | | |
| Mn | 0.06 | 0.21 | -0.04 | -0.14 | 1 | | |
| CIA | -0.62 | 0.55 | 0.70 | 0.37 | -0.07 | 1 | |
| V/Cr | -0.64 | 0.45 | 0.53 | 0.34 | -0.20 | 0.56 | 1 |

[a] The total number of samples used in this analysis is ~5000; $r$ values > 0.20 are significant at the 5% threshold (2$\sigma$); significant positive and negative correlations are shown in yellow and gray, respectively.

which entailed a 1.0-m upward adjustment of the GR profile in Fig. 5. As a consequence of this adjustment, the dark layers are seen to have higher GR signatures than the light layers, which is consistent with their higher TOC and clay-mineral content.

The origin of the meter-scale cycles in the 21.0-m interval of the Niuye-1 drillcore can be inferred based on the features described above. The darker layers show fine lamination, high TOC content, and high V/Cr ratios (a paleoredox proxy, e.g., Jones and Manning, 1994), which are consistent with more reducing conditions—probably euxinic given that benthic animals were largely excluded. In contrast, the lighter layers were deposited under oxic or suboxic conditions, as reflected in strong bioturbation, low TOC content, and low V/Cr ratios. In lacustrine systems, such redox variations are associated with changes in either frequency of water-column overturn, with darker layers deposited under more strongly stratified conditions (characteristic of humid-zone lakes, e.g., modern Lake Malawi; Brown et al., 2000), or in lake water level, with more reducing conditions during lake-level highstands (characteristic of arid-zone lakes, e.g., Triassic Newark Supergroup; Olsen, 2010). In both cases, more reducing conditions are generally linked to warmer, wetter climates (e.g., Cohen, 2003).

For the ~2-m cycles of the Shahejie Formation, the dark-colored layers in the middle of each cycle were probably formed during wet climate periods. Wet climate conditions contributed to higher paleoproductivity and reducing bottom-water conditions, as indicated by higher TOC and redox-sensitive trace-element concentrations (Fig. 5). Higher productivity may have been a result of enhanced chemical weathering fluxes during wet climate periods, and bottom-water anoxia would have been promoted by both higher organic carbon sinking fluxes and higher lake levels that favored a stratified water column (Zolitschka et al., 2015). In contrast, the light-colored layers in each cycle were probably formed during dry climate periods, which resulted in lower lake levels, reduced chemical weathering inputs, and diminished productivity (as reflected in lower TOC values) (Fig. 5). Light-colored layers are also characterized by peaks in calcite, which correlate with greater ostracod abundance. Ostracod abundance is 12–40 shells/cm$^2$ in the light-colored layers versus 0–1 shells/cm$^2$ in the dark-colored layers of the Shahejie Formation, a difference that was attributed to higher rates of preservation linked to dry climate conditions, higher evaporation, and relatively greater saturation of $CaCO_3$ in the lake water (Liu et al., 1994). The observation that a ~50% increase in TOC, quartz, and clay minerals is associated with a ~33% reduction in carbonate content in the darker layers relative to the lighter layers of the Shahejie Formation (see above) suggests that carbonate dilution (e.g., as a function of ostracod productivity or shell preservation potential) may have been the primary control on secular variation in sediment lithology within the Dongying lake basin.

Based on analysis of palynological assemblages, the mid-Eocene interval during which the Es$^4$ Member of the Shahejie Formation accumulated was characterized by a secular trend toward warmer and drier climate conditions, with an increase in the seasonality of precipitation toward the top of the unit (Hao et al., 2009; Wang et al., 2012). The shift toward drier conditions with increased seasonality is likely to have affected the hydrology of the Dongying lake basin, making it more susceptible to short-term climate trends that were recorded as sedimentary cycles (Fig. 5). The cyclicity of this core interval is sufficiently regular that a periodic controlling mechanism can be confidently inferred.

### 4.2. Spectral analysis of the GR profiles

The power spectra of the untuned GR profiles for the He-166 and SK-1 boreholes reveal hierarchies of distinct cycles. The Ed Formation to Es$^2$ Member yield peaks at wavelengths of ~130, 34, 16, 11, 9.7, 5.1, 4.4, 3.3, 2.8 m in the He-166 borehole (Fig. 7A), and at ~125, 59, 32, 13, 5.7, 4.1, 2.9, 2.4 m in the SK-1 borehole (Fig. 7B). The Es$^3$ Member yields peaks at wavelengths of ~122, 56, 30, 8.6 m in the He-166 borehole (Fig. 7C), and at ~80, 32, 22, 16, 10, 8.8, 3.8 m in the SK-1 borehole (Fig. 7D). The He-166 borehole did not extend deeper than the Es$^3$ Member. In the SK-1 borehole, the Es$^4$ Member yields peaks at wavelengths of ~71, 23, 17.6, 14.5, 11, 4.3, 3.3, 2.5 and 2.2 m (Fig. 7E), the Ek$^1$ to upper Ek$^2$ members yield peaks at wavelengths of ~100, 28, 22, 15, 7.4, 3.9, 3.1, and 2.9 m (Fig. 7F), and the lower Ek$^2$ Member yields peaks at wavelengths of ~110, 38, 26, 19, 10, 5.0, 4.2, 3.2, 2.6, and 2.4 m (Fig. 7G). The peaks at ~2–3 m in the Es$^3$ and Es$^4$ members (Fig. 7C, D, E) are weaker than those in the Ed Formation, Es$^2$ Member, and Ek Formation (Fig. 7A, B, F, G).

The power spectrum of the composite untuned GR profile for the entire Paleogene succession has significant peaks at ~114, 57–26, 16–10, 6.8–3.9, and 3.0–2.5 m (Fig. 8B). Given a total thickness of 6261.5 m and a duration of ~43 Ma (i.e., 66 to 23.0 Ma; Vandenberghe et al., 2012), the average accumulation rate for the Paleogene as a whole is 146 m Myr$^{-1}$. This rate yields tentative durations of 786 kyr and 391 kyr for the ~114-m and 57-m cycles, 100 to 69 kyr for the 16-m to 10-m cycles, 47 to 27 kyr for the 6.8-m to 3.9-m cycles, and 21 to 17 kyr for the 3.0-m to 2.5-m cycles. These periodicities correspond broadly to the 405-kyr long-eccentricity, the ~100-kyr short-eccentricity, the ~40-kyr obliquity, and the ~20-kyr precession orbital cycles, respectively. This correspondence indicates that the Eocene Dongying Depression lake was highly sensitive to climate fluctuations driven by orbital insolation variation.

### 4.3. Astronomical tuning of the composite GR record

Fig. 8A–B shows 100-kyr and 405-kyr components in the untuned time series of the composite GR series extracted by Gaussian band-pass filtering. These signals are readily apparent in the upper part of the Es$^4$ Member of the composite GR record, suggesting that the ~10-m and ~40-m cycles correspond to the short- and long-eccentricity orbital periodicities, respectively (Fig. 4). These filtered signals support our observational data from the upper part of the Es$^4$ Member in the Niuye-1 drillcore and imply that the ~2-m and ~10-m cycles correspond to the ~20-kyr precession and ~100-kyr short-eccentricity orbital periodicities (Fig. 5).

We identified 405-kyr cycles extracted by Gaussian bandpass filtering based on the above spectral analysis. We then tuned the ~57-m cycles to the 405-kyr long-eccentricity period to construct a ~42-Myr-long floating ATS (Fig. 8A). The power spectrum of the 405-kyr-tuned GR series reveals the presence of the predicted astronomical parameters: (1) a strong 405-kyr long-eccentricity peak and 131-kyr and 100-kyr short-eccentricity peaks, (2) 40.5-kyr, 38-kyr, and 37-kyr peaks

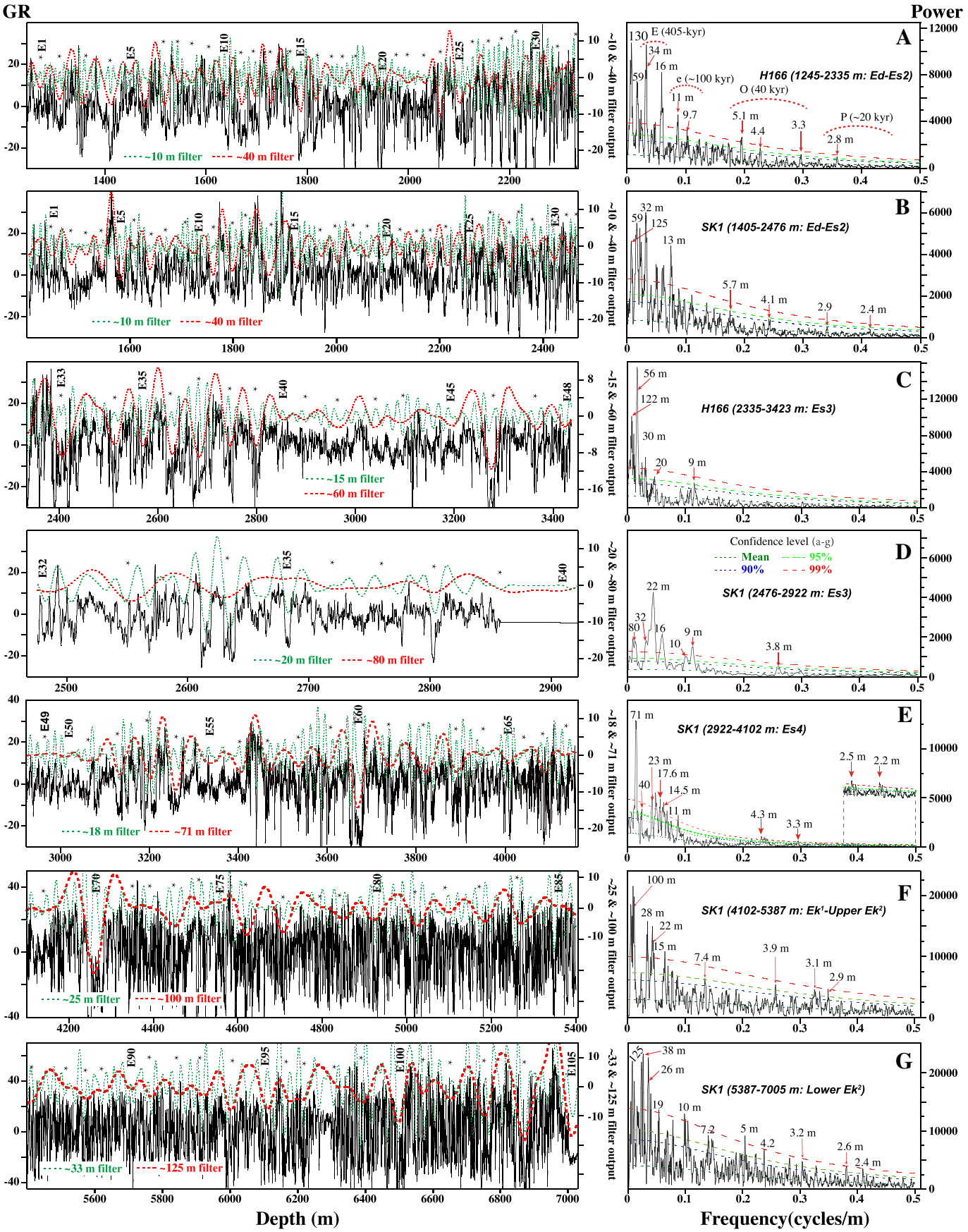


**Fig. 7.** GR series with ~100-kyr and ~405-kyr filter curves of the H-166 and SK-1 boreholes (left) and the 2π MTM (multitaper method) power spectrum (right) for the Ed Formation and $Es^2$ Member (1245–2335 m) of the H-166 borehole (A), Ed Formation and $Es^2$ Member (1405–2476 m) of the SK-1 borehole (B), $Es^3$ Member (2335–3423 m) of the H-166 borehole (C), $Es^3$ Member (2335–2922 m) of the SK-1 borehole (D), $Es^4$ Member (2922–4102 m) of the SK-1 borehole (E), $Ek^1$ and Upper $Ek^2$ members (4102–5387 m) of the SK-1 borehole (F), and lower $Ek^2$ Member (5387–7005 m) of SK-1 borehole (G). Asterisks (*) separate 405-kyr cycles.

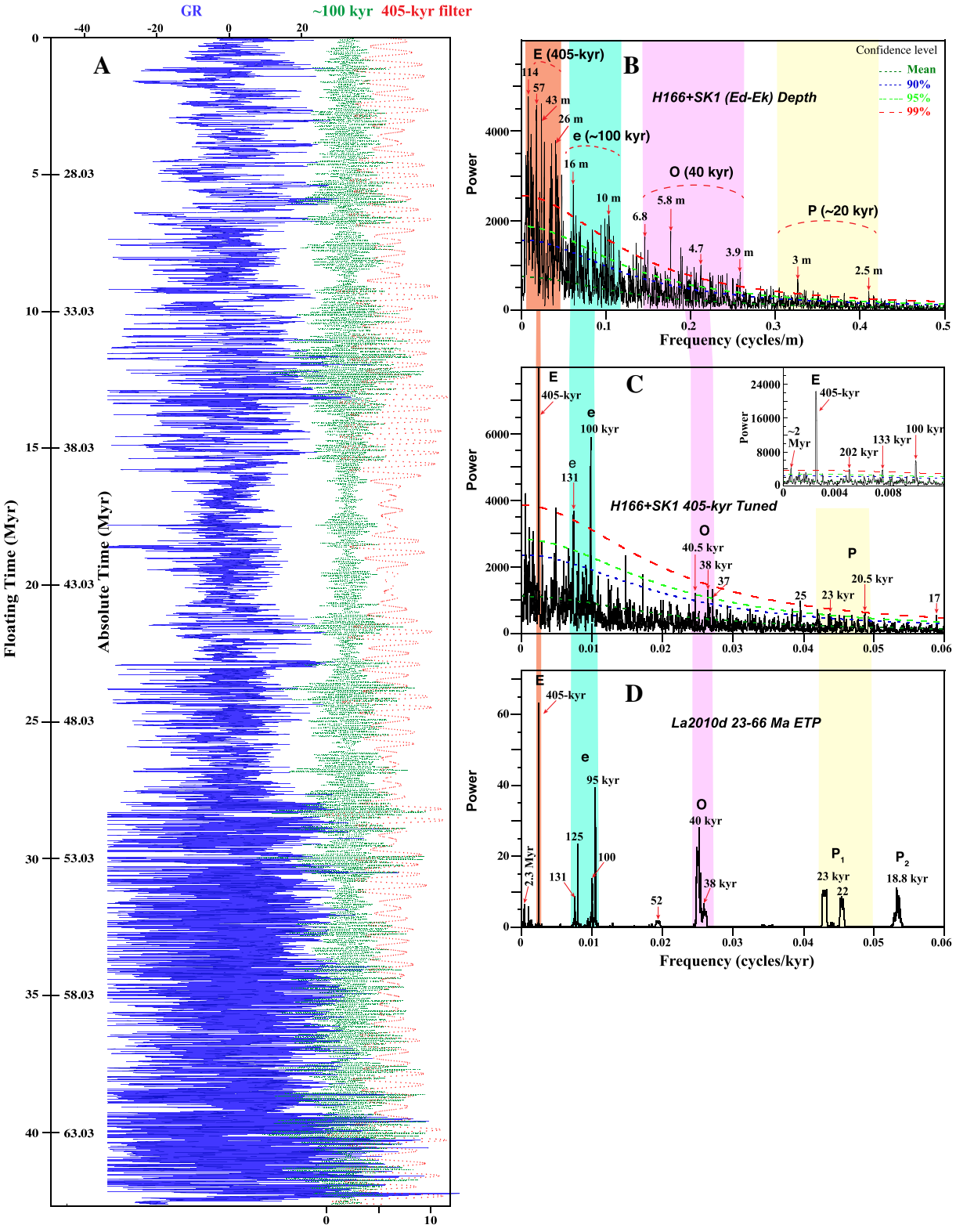


**Fig. 8.** The 405-kyr tuned GR series and power spectra. (A) 405-kyr tuned GR series with ~100-kyr and ~405-kyr filters, left time scale is floating, right is absolutely time scale when the top of Ed Member is anchored to the Paleogene-Neogene boundary as 23.03 Ma; (B) 2π MTM power spectrum of the composite section from the Ed Formation and $Es^3$ Member of well H-166 and the $Es^4$ Member and Ek Formation of well SK-1 in the depth domain; (C) power spectrum of the same units in the time domain; and (D) Earth's orbital parameters from 66 to 23 Ma presented in ETP format (Imbrie et al., 1984) according to the La2010d model (Laskar et al., 2011).

within the obliquity band, and (3) 23-kyr and 20.5-kyr peaks within the precession band (Fig. 8C). In addition, there is a peak at ~2 Myr that may correspond to the ~2.25-Myr ultra-long eccentricity cycle that has been identified in earlier studies (e.g., Hilgen et al., 1995; Gingerich, 2006; Lourens et al., 2005). These astronomical cycles are present above the 95% confidence level and compare well with the La2010d astronomical model (Fig. 8D; Laskar et al., 2011). The obliquity and precession index for the La2010d solution were calculated using the

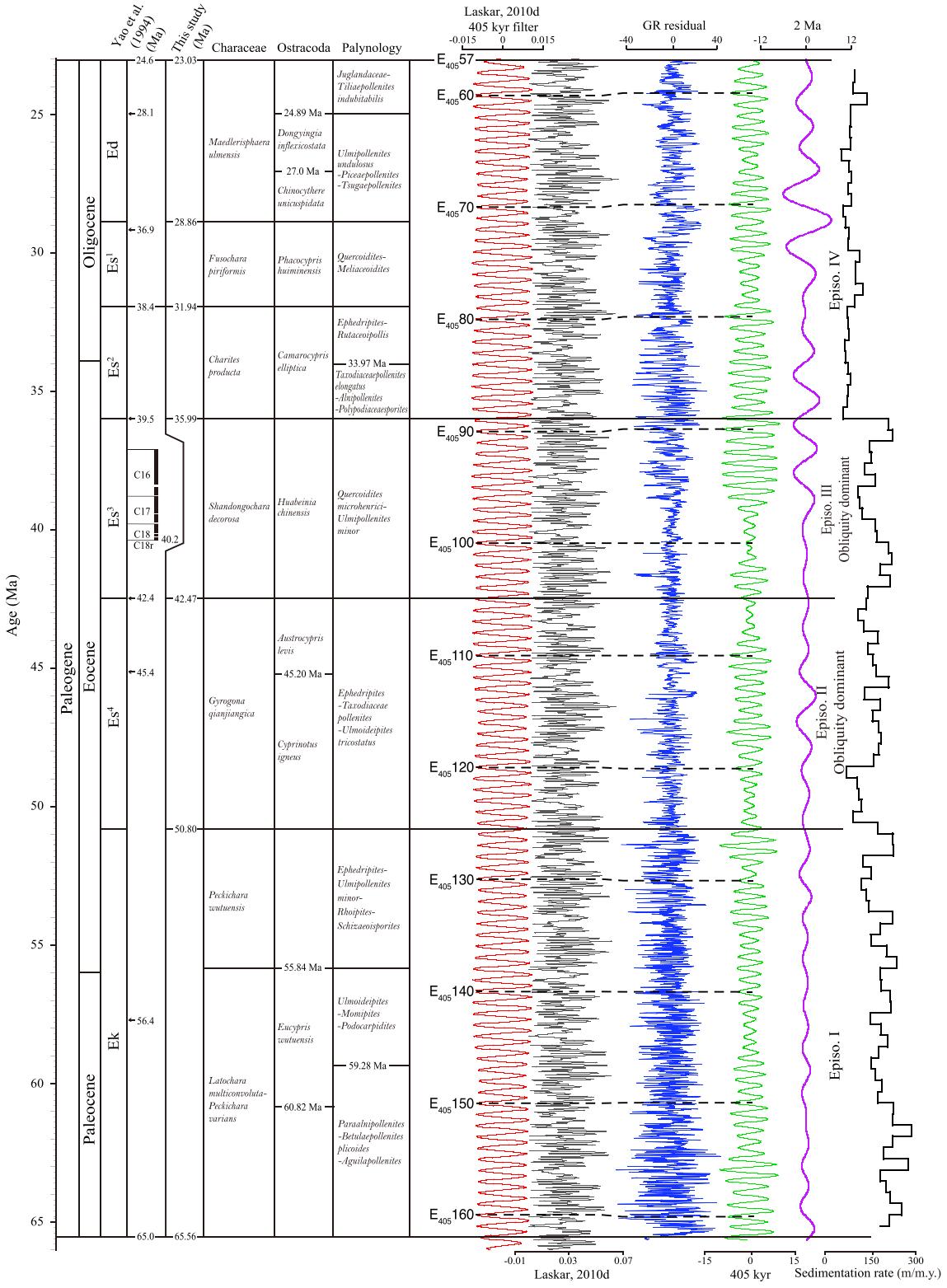


**Fig. 9.** Astronomical time scale (ATS) for the Paleogene succession of the Dongying Depression and comparison with the Yao et al. (1994) ages and recalibrated paleomagnetic polarity zone ages (according to the geomagnetic polarity time scale of GTS2012, Vandenberghe et al., 2012) for the BBB (left) and the Pacific oceanic plateau (POP) production rate (Larson, 1991) and the Southeast Indian Ridge (SEIR) spreading rate (Cande et al., 2010) (right).

procedure given in Appendix A of Wu et al. (2013). The La2010d ETP is a synthetic time series constructed from the sum of the normalized eccentricity (E), obliquity (T), and precession (P, where $P = e \times \sin(\Omega)$), which specifically predicts the 405-kyr long-eccentricity, 125-kyr and 95-kyr short-eccentricity, ~40-kyr obliquity, and 19-kyr and 23-kyr precession components as well as the ~2.25-Myr ultra-long eccentricity cycle during the time interval from 66 Ma to 23 Ma.

## 5. Discussion

### 5.1. An astronomical time scale (ATS) for the Paleogene

Because the Paleogene/Neogene boundary is well-dated (23.03 Ma; Gradstein et al., 2012) and regarded as conformable in the central Dongying Depression (Wu et al., 1998) (see Section 2.3), we adopted it as the anchor point for our floating ATS. This level corresponds to the 57th 405-kyr-eccentricity cycle ($E_{57}$) of the La2010d solution (Fig. 9). From this anchor point, our astronomical time scale (ATS) extends from the Paleogene/Neogene boundary at 23.03 Ma back to 65.56 Ma, i.e., close to the Cretaceous/Paleogene boundary (66.0 Ma), thus spanning the 57th to 162nd 405-kyr-eccentricity cycles ($E_{57}$-$E_{162}$) of the La2010d orbital record. Our results compare remarkably well with the La2010d eccentricity solution throughout the Paleogene (Fig. 9).

Our ATS for the Paleogene succession of the Jiyang Subbasin yields a total duration of 42.53 Myr (i.e., from 23.03 Ma to 65.56 Ma), which is compatible with the currently used timescale from 24.0 Ma to 65.0 Ma for this area (Yao et al., 1994, 2007; Hao et al., 2009; Feng et al., 2013) and also agrees well with the international Geologic Time Scale for the Paleogene Period (23.03 Ma to 66.0 Ma; Gradstein et al., 2012). In addition, our dates for epoch boundaries conform closely to those of the GTS2012 (unlike some of the dates in Yao et al., 1994, 2007). The Oligocene/Eocene boundary within the $Es^2$ Member was identified based on the Ephedripites-Rutaceoipollis/Taxodiaceaepollenites elongatus-Alnipollenites-Polypodiaceaesporites palynozones (RIPEDPCI, 1978c; Yao et al., 1994; Song, 1999) and corresponds to the 84.5th 405-kyr-eccentricity cycle of this study, the age of which in our ATS (33.97 Ma) matches closely the age of the Oligocene/Eocene boundary in the GTS2012 (33.9 Ma; Gradstein et al., 2012). The Eocene/Paleocene ($Ek^1$/$Ek^2$) boundary was identified based on the Ephedripites-Ulmipollenites minor-Rhoipites-Schizaeoisporites/Ulmoideipites-Momipites-Podocarpidites palynozones (RIPEDPCI, 1978c; Yao et al., 1994; Song, 1999) and corresponds to the 138th 405-kyr-eccentricity cycle of this study, the age of which in our ATS (55.84 Ma) matches closely the age of the Eocene/Paleocene boundary in the GTS2012 (56.0 Ma; Gradstein et al., 2012). These correspondences support the robustness of the Paleogene ATS developed in the present study, indicating that our revised geochronology for the Paleogene BBB is a considerable improvement over previously published versions.

Our results show little agreement with the BBB timescale of Yao et al. (1994), which is based on K-Ar dating of volcanic layers in the Liaohe Subbasin. In our anchored ATS, the age for the base of the Ed Formation is 28.86 Ma (Fig. 9), which is much younger than the K-Ar age of 36.9 Ma near the upper contact of $Es^1$. The ATS age of the base of $Es^1$ is 31.94 Ma, which is much younger than the K-Ar age of 38.4 Ma in the Liaohe Subbasin. The ATS calibrated age for the base of $Es^2$ is 35.99 Ma, which is much younger than the K-Ar age of 39.5 Ma. These large differences between the radiometric- and ATS-based ages may reflect problems with the K-Ar isotopic system (e.g., Min et al., 2000; Erwin, 2006; Kuiper et al., 2008), although other factors (e.g., differential fill rates between the Liaohe and Jiyang subbasins) might have played a role. Our ATS begins to converge with the timescale of Yao et al. (1994) around the base of the $Es^3$ Member, for which the calibrated ATS age is 42.47 Ma and the K-Ar age is 42.4 Ma. These age estimates are supported by magnetostratigraphic data, which yielded an estimate of ~43 Ma for the lower $Es^3$ Member at the C18n.1r/C18n.1n contact (Yao et al., 1994) based on the timescale of Harland et al. (1982). However, Yao et al. (2007) recalibrated the contact age of C18n.1r/C18n.1n as 38.975 Ma according to the GTS2004 (Ogg et al., 2004). In this study, according to the geomagnetic polarity time scale of GTS2012 (Vandenberghe et al., 2012), we update the top of the C18r magnetochron as 40.201 Ma. This updated age is consistent with our ATS age of the middle-lower $Es^3$ member (Fig. 9). The calibrated ATS age for the base of the $Es^4$ Member (50.8 Ma) is close to the age of 50.4 Ma proposed by Yao et al. (1994). The base of the Ek Formation, which corresponds to the base of the Paleogene, is estimated at 65.56 Ma in this study, which is close to the astronomically calibrated $^{40}Ar/^{39}Ar$ age of 65.95 Ma for the Cretaceous-Paleogene boundary (Kuiper et al., 2008) and the assigned age of 66.04 ± 0.05 Ma in GTS2012 (Vandenberghe et al., 2012).

### 5.2. Age calibration of Paleogene biozones and tectonic episodes of the BBB

The ATS established in this study is an independent and high-precision continuous time scale for the Paleogene succession in the Jiyang Subbasin, which can be used to calibrate biozones, sedimentation rates, and tectonic events of the BBB. Paleontological correlations have played a significant role in stratigraphic assignments within the Paleogene succession of the BBB. The most important fossil groups in this regard are the Characeae, Ostracoda, and palynomorphs (RIPEDPCI, 1978a, 1978b, 1978c; Yao et al., 1994). For example, the *Maedlerisphaera ulmensis*, *Fusochara piriformis*, and *Charites producta* characeaen zones mark the bases of the Ed, $Es^1$, and $Es^2$ members, respectively, in the Jiyang Subbasin (Figs. 2 and 9). Although widely used within the BBB and in other regions globally, these biozones have not been calibrated to any absolute reference time frame. The anchored ATS of this study provides absolute ages for biozones within the BBB. For example, the *Maedlerisphaera ulmensis* characeaen Zone in the Ed Formation has an age range of 28.86 Ma to 23.03 Ma, the *Huabeinia chinensis* ostracod Zone of the $Es^3$ Member an age range of 42.47 Ma to 35.99 Ma, and the *Ephedripites-Taxodiaceae pollenites-Ulmoideipites tricostatus* palynomorph Zone of the $Es^4$ Member an age range of 50.8 Ma to 42.47 Ma (Fig. 9; other biozone age ranges are also shown in this figure). This absolute age framework for biozones within the Paleogene succession of the BBB should prove useful for future stratigraphic correlation studies among the various basins of the BBB and, potentially, at a regional or global scale.

The four rifting episodes of the BBB were also recalibrated with more accurate time constraints based on our high-precision ATS (Fig. 9). Episode I (Ek Formation) extended from 65.56 Ma to 50.80 Ma, Episode II ($Es^4$ Member) from 50.8 Ma to 42.47 Ma, Episode III ($Es^3$ Member) from 42.47 Ma to 35.99 Ma, and Episode IV ($Es^2$-Ed) from 35.99 Ma to 23.03 Ma. Owing to the excellent conformity of our age model for the BBB with the international geologic time scale (GTS2012), these estimated ages for BBB rifting episodes are more accurate than previous estimates. Our age model revises the onset of Episode II to 50.80 Ma from the poorly constrained estimate of 56.4–45.4 Ma by Yao et al. (1994), and recalibrates the onset of Episode IV to 35.99 Ma from the earlier estimate of 39.5 Ma (Fig. 2). These revised ages permit a more accurate assessment of the relationship of BBB rifting episodes to regional climatic, tectonic, and magmatic events.

### 5.3. Paleoclimatic and tectonic events recorded in the Paleogene of the BBB

A long interval of global climatic cooling and drying commenced at the termination of the ~56.0-Ma Paleocene-Eocene Thermal Maximum (PETM) (Kennett and Stott, 1991; Jones et al., 2013) and continued until the Eocene-Oligocene boundary at 33.9 Ma, when the first Antarctic icesheet formed (Barker et al., 2007). This warming and drying climate transition is well-documented in mid-latitude regions of East Asia (Sluijs et al., 2006; Adams et al., 2011) including the BBB area (Hao et al., 2009; Wang et al., 2010; Feng et al., 2013; Li et al., 2014). It

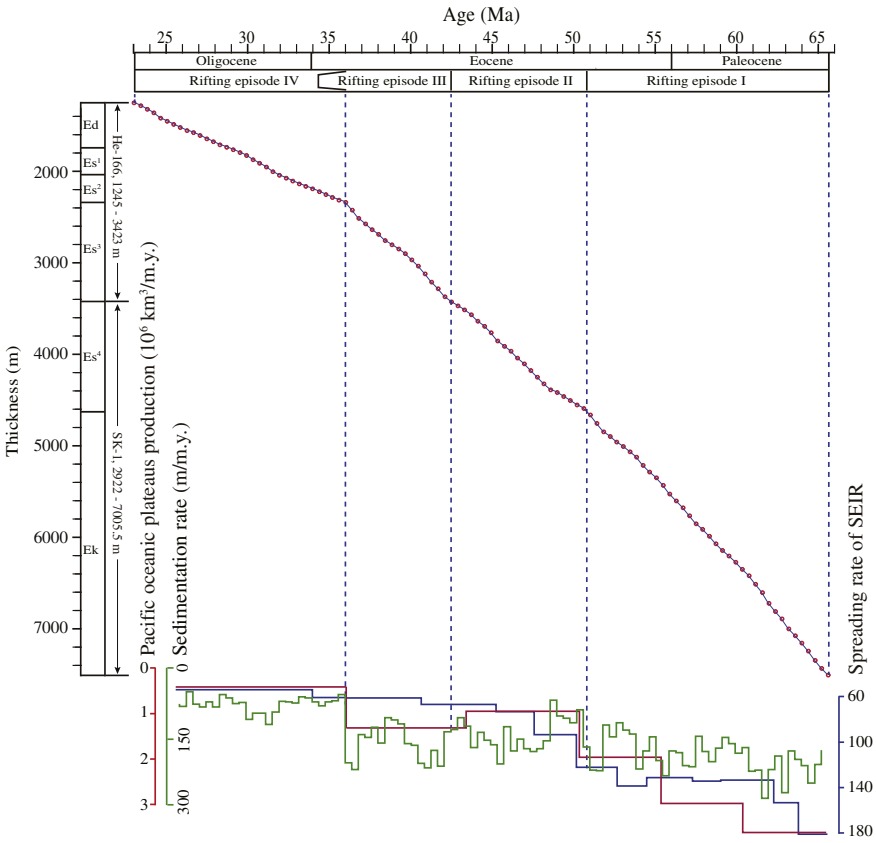


**Fig. 10.** Thickness-age diagram for the Paleogene succession of the Dongying Depression based on the ATS of the present study. Abbreviations: Ek, Kongdian Formation (Fm.); $Es^4$, $Es^3$, $Es^2$, and $Es^1$, fourth to first members of Shahejie Fm.; Ed, Dongying Fm. In the composite stratigraphic section, the interval 1245–3423 m (thickness of 2178 m) is based on the He-166 borehole, and the interval 3423–7506.5 m (thickness of 4083.5 m) is based on the SK-1 borehole, yielding a composite record of 6261.5 m in thickness.

is recorded in the Jiyang Subbasin as a succession of gypsiferous mudstones extending from the upper part of $Ek^1$ at ~5000 m to the top of $Es^4$ at ~2900 m in the SK-1 drillcore (Fig. 4). Warmer, drier conditions are also reflected in concurrent changes in spore-pollen floral communities in the BBB area (Hao et al., 2009). Based on our calibrated ATS, this warming phase ranged from 56.0 Ma to 42.5 Ma (Fig. 9). An important feature of this climate transition is a change in power spectral characteristics of the $Es^4$ and $Es^3$ members of the Shahejie Formation (Fig. 7A–G). Specifically, the ~6- to 4-m obliquity-band cycles of these members become stronger and the ~3- to 2-m precession-band cycles weaker relative to signals in older and younger strata of the SK-1 drillcore. We interpret this pattern to reflect a shift from dominant precession-eccentricity forcing to obliquity forcing of climate variation, which was possibly a contributing factor to (or a result of) the global Eocene cooling trend. A shift to dominant obliquity forcing in the early Eocene was also identified on the Demerara Rise in the west-central Atlantic (Westerhold and Röhl, 2009), suggesting that this orbital change had global consequences.

The recalibrated ages of the four rifting episodes of the BBB reveal important relationships to contemporaneous tectonic events at a regional to continental scale. In particular, the sediment accumulation rate profile bears strong similarities to production rates of Pacific oceanic plateaus (POP, Larson, 1991) and to spreading rates on the Southeast Indian Ridge (SEIR, Cande et al., 2010). High sedimentation rates during Episode I (65.56–50.80 Ma) correspond to maxima in both POP production and SEIR spreading rates, whereas moderate sedimentation rates during Episode II (50.8–42.47 Ma) and Episode III (42.47–35.99 Ma) correspond to a reduction in both POP production and SEIR spreading rates (Figs. 9 and 10; Larson, 1991; Cande et al., 2010). Low sedimentation rates during Episode IV (35.99–23.03 Ma) are consistent with minima in both POP production and SEIR spreading rates. Additionally, sharp decreases in sedimentation rates at the beginning of Episodes II and IV are matched by similar changes in POP production and SEIR spreading rates (Fig. 9).

Long-term changes in sedimentation rates of the Jiyang Subbasin indicate that the history of tectonic subsidence and sedimentary filling of the depocenter of the BBB was significantly influenced by the subduction of the Pacific Plate along the eastern margin of Asia (Northrup et al., 1995) and the collision of the Indian Plate with the Eurasian Plate (Tapponnier et al., 1982). The slab pull of the Pacific Plate and far-field stresses from the India-Eurasia collision are likely to have induced secular variation in the crustal stress field around the BBB, leading to episodic rifting and subsidence (Khain, 1992; Ziegler and Cloetingh, 2004) and, thus, in the generation of basinal accommodation space (Catuneanu, 2002). Concurrently, uplift of surrounding crustal blocks and graben shoulders would have increased erosion and siliciclastic inputs into the BBB. The rapid rate of subsidence of the BBB during the Paleogene (~130 m $Myr^{-1}$) reflects the importance of these processes.

## 6. Conclusions

Natural gamma-ray logging data from the He-166 and SK-1 drillcores, which penetrated the full Paleogene succession of the Jiyang Subbasin of the Bohai Bay Basin, reveal an unusually regular record of orbital forcing of sedimentation within this lacustrine succession. Based on these records, we constructed an astronomical time scale (ATS) in which the 405-kyr long-eccentricity cycles correspond well to the long-eccentricity model of the La2010d orbital solution. This ATS represents a continuous, high-resolution, and absolute time scale for the Paleogene stratigraphic succession of the Jiyang Subbasin that is a major improvement on earlier age models for the BBB. Based on our ATS, we calculated sedimentation rates within the Jiyang Subbasin and refined the durations and boundary ages of biozones and basinal rifting episodes of the BBB, providing a robust geochronological framework for future studies in this region.

Our new age model provides a basis for re-evaluation of the evolutionary history of the BBB, as well as for an improved understanding of its connections to regional climatic, tectonic, and magmatic events.

The recalibrated rifting episodes show a close relationship to the production rate of Pacific oceanic plateaus and to spreading rates of the Southeast Indian Ridge system. These observations indicate that subsidence of the BBB was strongly influenced by subduction of the Pacific Plate along the eastern margin of Asia and by the collision of the Indian and Eurasian plates. Furthermore, the evaporite deposits in the $Ek^1$ and $Es^4$ members of the SK-1 borehole and an analysis of climatic controls on meter-scale cyclicity in the $Es^3$ Member confirm that a climatic drying trend developed in mid-latitude regions of East Asia during the Eocene.

## Acknowledgments

We thank the Shengli Oilfield Company of SINOPEC for providing drillcore samples and GR logging data. The study data are available in Excel format at https://www.dropbox.com/sh/hijfrop62vmo65z/AABMaKg9WqLe5EgzPHXHZ4nIa?dl=0. We thank David De Vleeschouwer and Youliang Feng for insightful reviews of the manuscript, and Zhongshi Zhang for editorial handling of the manuscript. We also thank Dr. Xiaofeng Liu for his helpful discussion, and CUG and SINOPEC team members for their work on the Eastern China Paleogene Lacustrine Shale Oil project. Research by ZHL and CJH is supported by NSFC program (No. 41772148, 41772029, 41202087and 41322013), National Key Basic Research program 2016ZX05060-004, 2014CB239100, the 111 Projects (No. B14031 and B08030), Natural Science Foundation for Distinguished Young Scholars of Hubei Province of China (2016CFA051), and China Geological Survey program 12120114046601. Research by TJA is supported by the U.S. National Science Foundation (Sedimentary Geology and Paleobiology program), the NASA Exobiology program, and the China University of Geosciences-Wuhan (SKL-GPMR program GPMR201301, and SKL-BGEG program BGL201407).

## References

Abels, H.A., Abdul, A.H., Krijgsman, W., Smeets, S.J.B., Hilgen, F.J., 2010. Long- period eccentricity control on sedimentary sequences in the continental Madrid Basin (middle Miocene, Spain). Earth Planet. Sci. Lett. 289, 220–231.

Adams, J.S., Kraus, M.J., Wing, S.L., 2011. Evaluating the use of weathering indices for determining mean annual precipitation in the ancient stratigraphic record. Palaeogeogr. Palaeoclimatol. Palaeoecol. 3-4, 358–366.

Barker, P.F., Diekmann, B., Escutia, C., 2007. Onset of Cenozoic Antarctic glaciation. Deep-Sea Res. II Top. Stud. Oceanogr. 54, 2293–2307.

Brown, E.T., Le Callonnec, L., German, C.R., 2000. Geochemical cycling of redox-sensitive metals in sediments from Lake Malawi: a diagnostic paleotracer for episodic changes in mixing depth. Geochim. Cosmochim. Acta 64, 3515–3523.

Cande, S.C., Patriat, P., Dyment, J., 2010. Motion between the Indian, Antarctic and African plates in the early Cenozoic. Geophys. J. Int. 183, 127–149.

Catuneanu, O., 2002. Sequence stratigraphy of clastic systems: concepts, merits, and pitfalls. J. Afr. Earth Sci. 35, 1–43.

Chen, S., Liu, X., Cui, Y., Zhao, X., Zhang, J., 2017. Palaeogene structural evolution of Dongying Depression, Bohai Bay Basin, NE China. Int. Geol. Rev. 59, 259–273.

Cohen, A.S., 2003. Paleolimnology: The History and Evolution of Lake Systems. Oxford University Press, Oxford, pp. 528.

Erwin, D.H., 2006. Dates and rates: temporal resolution in the deep time stratigraphic record. Annu. Rev. Earth Planet. Sci. 34, 569–590.

Feng, Y., Li, S., Lu, Y., 2013. Sequence stratigraphy and architectural variability in Late Eocene lacustrine strata of the Dongying Depression, Bohai Bay Basin, eastern China. Sediment. Geol. 295, 1–26.

Ghil, M., Allen, M.R., Dettinger, M.D., Ide, K., Kondrashov, D., Mann, M.E., Robertson, A.W., Saunders, A., Tian, Y., Varadi, F., Yiou, P., 2002. Advanced spectral methods for climatic time series. Rev. Geophys. 40, 41 (art. 3).

Gingerich, P.D., 2006. Environment and evolution through the Paleocene-Eocene thermal maximum. Trends Ecol. Evol. 21, 246–253.

Gradstein, F.M., Ogg, J.G., Schmitz, M., Ogg, G. (Eds.), 2012. The Geologic Time Scale 2012. Elsevier, Amsterdam (2 vols).

Guo, X., Liu, K., He, S., Song, G., Wang, Y., Hao, X., Wang, B., 2012. Petroleum generation and charge history of the northern Dongying Depression, Bohai Bay Basin, China: insight from integrated fluid inclusion analysis and basin modeling. Mar. Pet. Geol. 32, 21–35.

Hao, F., Zhou, X., Zhu, Y., Yang, Y., 2009. Mechanisms for oil depletion and enrichment on the Shijiutuo uplift, Bohai Bay Basin, China. Am. Assoc. Pet. Geol. Bull. 93, 1015–1037.

Hao, H., Ferguson, D.K., Feng, G.P., Ablaev, A., Wang, Y.F., Li, C.S., 2010. Early Paleocene vegetation and climate in Jiayin, NE China. Clim. Chang. 99, 547–566.

Harland, W.B., Cox, A.V., Llewellyn, P.G., Pickton, C.A.G., Smith, A.G., Walters, R., 1982. A Geologic Time Scale. Cambridge University Press, New York, pp. 131.

Hennekam, R., de Lange, G., 2012. X-ray fluorescence core scanning of wet marine sediments: methods to improve quality and reproducibility of high-resolution paleoenvironmental records. Limnol. Oceanogr. Methods 10, 991–1003.

Hilgen, F.J., Krijgsman, W., Langereis, C.G., Lourens, L.J., Santarelli, A., Zachariasse, W.J., 1995. Extending the astronomical (polarity) time scale into the Miocene. Earth Planet. Sci. Lett. 136, 495–510.

Hinnov, L.A., Hilgen, F.J., 2012. Cyclostratigraphy and astrochronology. In: Gradstein, F.M., Ogg, J.G., Schmitz, M., Ogg, G. (Eds.), The Geologic Time Scale 2012. Elsevier, Amsterdam, pp. 63–83.

Huang, L., Liu, C., Wang, Y., Zhao, J., Mountney, N.P., 2014. Neogene–Quaternary postrift tectonic reactivation of the Bohai Bay Basin, eastern China. Am. Assoc. Pet. Geol. Bull. 98, 1377–1400.

Imbrie, J., Hays, J.D., Martinson, D.G., McIntyre, A., Mix, A.C., Morley, J.J., Pisias, N.G., Prell, W.L., Shackleton, N.J., 1984. The orbital theory of Pleistocene climate: support from a revised chronology of the marine d18O record. In: Berger, A.L. (Ed.), Milankovitch and Climate, Part 1. D. Reidel Publishing Company, pp. 269–305.

Jones, B., Manning, D.A., 1994. Comparison of geochemical indices used for the interpretation of palaeoredox conditions in ancient mudstones. Chem. Geol. 111, 111–129.

Jones, T.D., Lunt, D.J., Schmidt, D.N., Ridgwell, A., Sluijs, A., Valdes, P.J., Maslin, M., 2013. Climate model and proxy data constraints on ocean warming across the Paleocene–Eocene Thermal Maximum. Earth Sci. Rev. 125, 123–145.

Kennett, J.P., Stott, L.D., 1991. Abrupt deep-sea warming, palaeoceanographic changes and benthic extinctions at the end of the Palaeocene. Nature 353, 225–229.

Khain, V.Y., 1992. The role of rifting in the evolution of the Earth's crust. Tectonophysics 215, 1–7.

Kuiper, K.F., Deino, A., Hilgen, F.J., Krijgsman, W., Renne, P.R., Wijbrans, J.R., 2008. Synchronizing rock clocks of earth history. Science 320, 500–504.

Larson, R.L., 1991. Latest pulse of Earth: evidence for a mid-Cretaceous superplume. Geology 19, 547–550.

Laskar, J., Fienga, A., Gastineau, M., Manche, H., 2011. La2010: a new orbital solution for the long-term motion of the Earth. Astron. Astrophys. 532, A89 (17 pp).

Li, G., Wang, Y., Lu, Z., Liao, W., Song, G., Wang, X., Xu, X., 2014. Geobiological processes of the formation of lacustrine source rock in Paleogene. Science China Earth Sciences 5, 976–987.

Lin, C.S., Zheng, H.R., Ren, J.Y., Liu, J.Y., Qiu, Y.G., 2004. The control of syn-depositional faulting on the Eogene sedimentary basin fills of the Dongying and Zhanhua sags, Bohai Bay basin. Sci. China. Ser. D. 47, 769–782.

Liu, C., Ding, L., Hong, T., Bi, H., Zhao, Q., 1994. Nonuniformity in abundance of ostracoda from Early Tertiary Shahejie Formation in the Dongying depression, Shandong and their geological significance. Acta Microbiol Sin. 2, 213–222 (in Chinese).

Liu, M., Cui, X., Liu, F., 2004. Cenozoic rifting and volcanism in eastern China: a mantle dynamic link to the Indo-Asian collision? Tectonophysics 393, 29–42.

Lourens, L.J., Sluijs, A., Kroon, D., Zachos, J.C., 2005. Astronomical pacing of late Palaeocene to early Eocene global warming events. Nature 435, 1083–1087.

Machlus, M.L., Olsen, P.E., Christie-Blick, N., Hemming, S.R., 2008. Spectral analysis of the lower Eocene Wilkins Peak Member, Green River Formation, Wyoming: support for Milankovitch cyclicity. Earth Planet. Sci. Lett. 268, 64–75.

Mann, M.E., Lees, J.M., 1996. Robust estimation of background noise and signal detection in climatic time series. Clim. Chang. 33, 409–445.

Min, K., Mundil, R., Renne, P.R., Ludwig, K.R., 2000. A test for systematic errors in $^{40}Ar/^{39}Ar$ geochronology through comparison with U/Pb analysis of a 1.1-Ga rhyolite. Geochim. Cosmochim. Acta 64, 73–98.

Nesbitt, H.W., Young, G.M., 1982. Early Proterozoic climates and plate motions inferred from major element chemistry of lutites. Nature 299, 715–717.

Northrup, C.J., Royden, L.H., Burchfiel, B.C., 1995. Motion of the Pacific plate relative to Eurasia and its potential relation to Cenozoic extension along the eastern margin of Eurasia. Geology 23, 719–722.

Ogg, J.G., Agterberg, F.P., Gradstein, F.M., 2004. A geologic time scale 2004. In: Abstracts with Programs-Geological Society of America. 36. pp. 74.

Ogg, J.G., Smith, A.G., 2005. The geomagnetic polarity time scale. In: Gradstein, F.M., Ogg, J.G., Smith, A.G. (Eds.), A Geologic Time Scale 2004. Cambridge University Press, Cambridge, pp. 63–86.

Olsen, P.E., 2010. Fossil great lakes of the Newark Supergroup–30 years later. In: Field Trip Guidebook. New York State Geological Association, 83rd Annual Meetingpp. 101–163.

Olsen, P.E., Kent, D.V., 1996. Milankovitch climate forcing in the tropics of Pangea during the Late Triassic. Palaeogeogr. Palaeoclimatol. Palaeoecol. 122, 1–26.

Paillard, D., Labeyrie, L., Yiou, P., 1996. Macintosh program performs time-series analysis. EOS Trans. Am. Geophys. Union 77, 379.

Petroleum Geology Group of Shengli Oilfield, 1993. Petroleum Geology of China. Vol. 6 Petroleum Industry Press, Beijing (518 pp, in Chinese).

Postma, G., Ten Veen, J.H., 1999. Astronomically and tectonically linked variations in gamma-ray intensity in Late Miocene hemipelagic successions of the Eastern Mediterranean Basin. Sediment. Geol. 128, 1–12.

Preto, N., Hinnov, L.A., 2003. Unraveling the origin of carbonate platform cyclothems in the Upper Triassic Durrenstein Formation (Dolomites, Italy). J. Sediment. Res. 73, 774–789.

Price, J.R., Velbel, M.A., 2003. Chemical weathering indices applied to weathering profiles developed on heterogeneous felsic metamorphic parent rocks. Chem. Geol. 202, 397–416.

Prokoph, A., Villeneuve, M., Agterberg, F.P., Rachold, V., 2001. Geochronology and calibration of global Milankovitch cyclicity at the Cenomanian-Turonian boundary.

Geology 29, 523–526.
Qi, J., Yang, Q., 2010. Cenozoic structural deformation and dynamic processes of the Bohai Bay basin province, China. Mar. Pet. Geol. 27, 757–771.
RIPEDPCI (Research Institute of Petroleum Exploration and Development of Petroleum Chemical Industry), 1978a. Early Tertiary Ostracods in Bohai Coastal Area. Science Press, Beijing (205 pp, in Chinese).
RIPEDPCI (Research Institute of Petroleum Exploration and Development of Petroleum Chemical Industry), 1978b. Early Tertiary Charophytes in Bohai Coastal Area. Science Press, Beijing (49 pp., in Chinese).
RIPEDPCI (Research Institute of Petroleum Exploration and Development of Petroleum Chemical Industry), 1978c. Early Tertiary Sporopollens in Bohai Coastal Area. Science Press, Beijing (177 pp., in Chinese).
Ruhl, M., Deenen, M.H.L., Abels, H.A., Bonis, N.R., Krijgsman, W., Kürschner, W.M., 2010. Astronomical constraints on the duration of the early Jurassic Hettangian stage and recovery rates following the end-Triassic mass extinction (St Audrie's Bay/East Quantoxhead, UK). Earth Planet. Sci. Lett. 295, 262–276.
Schnyder, J., Ruffell, A., Deconinck, J.F., Baudin, F., 2006. Conjunctive use of spectral gamma-ray logs and clay mineralogy in defining late Jurassic–early Cretaceous palaeoclimate change (Dorset, UK). Palaeogeogr. Palaeoclimatol. Palaeoecol. 229, 303–320.
Sluijs, A., Schouten, S., Pagani, M., Woltering, M., Brinkhuis, H., Damsté, J.S.S., Dickens, G.R., Huber, M., Reichart, G.J., Stein, R., Matthiessen, J., 2006. Subtropical Arctic Ocean temperatures during the Palaeocene/Eocene thermal maximum. Nature 441, 610–613.
Song, Z.C., 1999. Fossil Spores and Pollen of China. In: Late Cretaceous and Tertiary Spores and Pollen. Vol. 1 China Science Press, Beijing (1117 pp., in Chinese).
Strasser, A., Hilgen, F.J., Heckel, P.H., 2006. Cyclostratigraphy–concepts, definitions, and applications. Newsl. Stratigr. 42, 75–114.
Tapponnier, P., Peltzer, G., Le Dain, A.Y., Armijo, R., Cobbold, P., 1982. Propagating extrusion tectonics in Asia: new insights from simple experiments with plasticine. Geology 10, 611–616.
Thomson, D.J., 1982. Spectrum estimation and harmonic analysis. Proc. IEEE 70, 1055–1096.
Van Vugt, N., Langereis, C.G., Hilgen, F.J., 2001. Orbital forcing in Pliocene–Pleistocene Mediterranean lacustrine deposits: dominant expression of eccentricity versus precession. Palaeogeogr. Palaeoclimatol. Palaeoecol. 172, 193–205.
Vandenberghe, N., Hilgen, F.J., Speijer, R.P., 2012. The paleogene period. In: Gradstein, F.M., Ogg, J.G., Schmitz, M., Ogg, G. (Eds.), The Geologic Time Scale 2012. Vol. 2. Elsevier, Amsterdam, pp. 855–921.
Wang, Q., Ferguson, D.K., Feng, G.P., Ablaev, A.G., Wang, Y.F., Yang, J., Li, Y.L., Li, C.S., 2010. Climatic change during the Palaeocene to Eocene based on fossil plants from Fushun, China. Palaeogeogr. Palaeoclimatol. Palaeoecol. 295, 323–331.
Wang, C., He, Z., Li, H., Zhang, C., He, Q., 2012. Paleogene palynological assemblages in the Western Qingdong sag, Shanhong Province and their significance. Acta Microbiol Sin. 29, 70–79 (in Chinese with English abstract).
Westerhold, T., Röhl, U., 2009. High resolution cyclostratigraphy of the early Eocene–new insights into the origin of the Cenozoic cooling trend. Clim. Past 5, 309–327.
Wu, Z.P., Shi, B.Q., Zhou, Y.Q., Li, J.M., 1998. A study on hiatus surface of Neogene-Eogene in Jiyang Depression. Oil Gas Geol. 19, 313–317 (in Chinese with English abstract).
Wu, H., Zhang, S., Jiang, G., Huang, Q., 2009. The floating astronomical time scale for the terrestrial Late Cretaceous Qingshankou Formation from the Songliao Basin of Northeast China and its stratigraphic and paleoclimate implications. Earth Planet. Sci. Lett. 278, 308–323.
Wu, H., Zhang, S., Jiang, G., Hinnov, L., Yang, T., Li, H., Wan, X., Wang, C., 2013. Astrochronology of the early Turonian–early Campanian terrestrial succession in the Songliao Basin, northeastern China and its implication for long-period behavior of the Solar System. Palaeogeogr. Palaeoclimatol. Palaeoecol. 385, 55–70.
Wu, H., Zhang, S., Hinnov, L.A., Jiang, G., Yang, T., Li, H., Wan, X., Wang, C., 2014. Cyclostratigraphy and orbital tuning of the terrestrial upper Santonian–lower Danian in Songliao Basin, northeastern China. Earth Planet. Sci. Lett. 407, 82–95.
Yao, Y.M., Liang, H.D., Cai, Z.G., 1994. Tertiary in Petroliferous Regions of China: IV, The Bohai Gulf Basin. Petroleum Industry Press, Beijing (240 pp., in Chinese).
Yao, Y.M., Xu, D.Y., Li, B.L., Zhang, H.F., Zhang, S.P., Yao, S., 2007. High resolution cyclostratigraphic study on the third Member of Shahejie Formation of drill core Niu38 in the Dongying Depression, Shandong Province. J. Stratigr. 31, 229–239 (in Chinese with English abstract).
Zhang, S.W., 2004. The application of an integrated approach in exploration of lacustrine turbidites in Jiyang Sub-basin, Bohai Bay Basin, China. J. Pet. Sci. Eng. 41, 67–77.
Ziegler, P.A., Cloetingh, S., 2004. Dynamic processes controlling evolution of rifted basins. Earth Sci. Rev. 64, 1–50.
Zolitschka, B., Francus, P., Ojala, A.E.K., Schimmelmann, A., 2015. Varves in lake sediments–a review. Quat. Sci. Rev. 117, 1–41.